

Modeling and Analysis of a Novel Pneumatic Artificial Muscle and Pneumatic Arm Exoskeleton

Hee Doo Yang

Dissertation submitted to the Faculty of the
Virginia Polytechnic Institute and State University
in partial fulfillment of the requirements for the degree of

Master of Science
in
Mechanical Engineering

Alan T. Asbeck, Chair
Alfred L. Wicks
Reza Mirzaeifar

May 1, 2017
Blacksburg, Virginia

Keywords: pneumatic muscles, textile actuators, soft actuators, pneumatic exoskeletons,
soft robotics

Copyright 2017, Hee Doo Yang

Modeling and Analysis of a Novel Pneumatic Artificial Muscle and Pneumatic Arm Exoskeleton

Hee Doo Yang

(ABSTRACT)

The soft robotics field is developing rapidly and is poised to have a wide impact in a variety of applications. Soft robots have intrinsic compliance, offering a number of benefits as compared to traditional rigid robots. Compliance can provide compatibility with biological systems such as the human body and can provide some benefits for human safety and control. Further research into soft robots can be advanced by further development of pneumatic actuators.

Pneumatic actuators are a good fit for exoskeleton robots because of their light weight, small size, and flexible materials. This is because a wearable robot should be human friendly, therefore, it should be light weight, slim, powerful, and simple.

In this paper, a novel pneumatic artificial muscle using soft materials including integrated electronics for wearable exoskeletons is proposed. We describe the design, fabrication, and evaluation of the actuator, as well as the manufacturing process used to create it. Compared to traditional pneumatic muscle actuators such as the McKibben actuator and new soft actuators that were recently proposed, the novel actuator overcomes shortcomings of prior work. This is due to the actuator's very high contraction ratio that can be controlled by the manufacturing process. In this paper, we describe the design, fabrication, and evaluation of a novel pneumatic actuator that can accommodate integrated electronics for displacement

and pressure measurements used for data analysis and control. The desired performance characteristics for the actuator were $100 \sim 400\text{N}$ at between 35kPa and 105kPa , and upon testing we found almost $120 \sim 300\text{N}$ which confirms that these actuators may be suitable in soft exoskeleton applications with power requirements comparable to rigid exoskeletons.

Furthermore, a novel soft pneumatic elbow exoskeleton based on the pneumatic actuator concept and manufacturing process is presented. Each structure is designed and manufactured with all fabric. The distally-worn structure is only 300g , which is light weight for an arm exoskeleton, and the design is simple, leading to a low materials cost.

Modeling and Analysis of a Novel Pneumatic Artificial Muscle and Pneumatic Arm Exoskeleton

Hee Doo Yang

(GENERAL AUDIENCE ABSTRACT)

The soft robotics field is developing rapidly and is poised to have a wide impact in a variety of applications. The soft robotics is the specific field of robotics, which deals with flexible materials and different geometry in contrast to general robots made by rigid materials. Therefore, soft robots have intrinsic compliance, offering a number of benefits as compared to traditional rigid robots. Compliance can provide compatibility with biological systems such as the human body and can provide some benefits for human safety and control. Further research into soft robots can be advanced by the further development of pneumatic actuators.

Pneumatic actuators are a good fit for exoskeleton robots because of their light weight, small size, and flexible materials. This is because a wearable robot should be human-friendly, therefore, it should be light weight, slim, powerful, and simple.

In this paper, a novel pneumatic artificial muscle using soft materials for wearable exoskeletons is proposed. We describe the design, fabrication, and evaluation of the actuator, as well as the manufacturing process used to create it and its electronic system for data analysis and control.

Furthermore, a novel soft pneumatic elbow exoskeleton based on the pneumatic actuator concept and manufacturing process is presented. Each structure is designed and manufac-

tured with all fabric. The distally-worn structure is only 300g, which is light weight for an arm exoskeleton, and the design is simple, leading to a low materials cost.

Acknowledgments

I would like to express my sincere appreciation to my advisor, Dr. Alan T. Asbeck, who gave me this opportunity. Over the past two years, I have received invaluable guidance and inspiration from Dr. Alan Asbeck. The rigorous approach toward research and critical thinking I learned from him will provide lasting benefits throughout my future career.

I also would like to thank Dr. Alfred Wicks, and Dr. Reza Mirzaeifar for serving on my advisory committee and providing me academic and professional suggestions. Hopefully, there will be more opportunities to discuss future research projects with them.

I am particularly indebted to my family. My parents have always supported my choices in every step of my life. Sang Yong Yang, I am proud of having you as my father. Mi Hyun Park, I am honored to be your son. And finally, Ah Jung Yang, I thank you for being my rival in good faith. You have helped me achieve the goals I once believed were unattainable.

Contents

1	Introduction	1
2	Modeling and Analysis of a novel pneumatic artificial muscle	6
2.1	Abstract	6
2.2	Introduction	7
2.3	Overview	18
2.4	Materials and Methods	22
2.4.1	Fabrication Methods	22
2.4.2	Actuator Modeling	23
2.5	Results and Discussion	28
2.5.1	Experimental Evaluation	28
2.5.2	Electronics Integration and Evaluation	34

3 Pneumatic Elbow Exoskeleton	41
4 Conclusion	48
5 Bibliography	50

List of Figures

1.1	An exoskeleton robot for assisting rehabilitation of arm functions [1].	2
1.2	A Self-Contained Transfemoral prosthesis leg [2].	2
1.3	University of California at Berkeley's BLEEX exoskeleton [3].	3
1.4	Pneumatic robotic arm made from textiles [4].	4
1.5	A pneumatic arm exoskeleton made by Otherlab [5].	5
2.1	A classification framework for the different types of actuators, Class I : Peano muscle / Flat PAM, McKibben Muscle / PPAM and Our Actuator, Class II: VAMPs and Bellows textile muscle, Class III: Fast Pneu-nets actuator and our inner actuator.	8
2.2	The McKibben actuator.	10
2.3	Pleated pneumatic artificial muscles(PPAM).	11
2.4	A peano-fluidic muscle.	12

2.5 A schematic figure of the operating principle of mechanisms that contract when expanded horizontally, assuming a constant edge length. (a) Traditional pneumatic actuators start out tall and thin and contract to become more cylindrical or spherical. (b) Greater changes in length can be achieved if the final state can be a wide rectangle instead of a circle. The pneumatic actuator developed in this paper uses this structure.	13
2.6 A Bellows textile muscle [6].	14
2.7 Vacuum-Actuated Muscle-inspired Pneumatic structures (VAMPs) [7]. . . .	15
2.8 The Fast Pneu-Nets actuator (fPN) [8, 9].	16
2.9 The concept of the actuator: (a) Initial state of actuator prototype, (b) Initial state of actuator model, (c) Final state of actuator prototype, (d) Final state of actuator model, (e) Inner actuators, (f) Outer actuators.	19
2.10 The concept of the actuator including integrated electronics (a) Actuator prototype, (b) The first thin plastic structure embedding an LED board, (c) The second plastic structure attaching a displacement sensor and a pressure sensor.	21
2.11 The manufacturing process of the actuator: Steps 1, 2, and 3 are for the fabrication of the inner actuator, and steps 4, and 5 are for the fabrication of the outer actuator.	23

2.12 The mathematical models of the actuator, (a) The diagram of the actuator, (b) The inner structure of the actuator, and (c) A single unit of the inner actuator.	24
2.13 Simulation of the volume versus displacement of a single chamber in the inner actuator using the model in Figure 2.5, for sample lengths of $y=4\text{cm}$, $f=3\text{cm}$, $g=3\text{cm}$ and $e=1\text{cm}$	27
2.14 Typical static force operated by the actuator in function of the contraction ratio and comparison between two various size of the actuator (a) The property at typical pressure (34.5kPa) (b) The property at typical pressure (69kPa). .	30
2.15 Typical static force operated by the actuator in function of the contraction ratio and comparison the force regarding various pressure ranges (a) The property of the actuator($y : l = 2 : 5$) (b) The property of the actuator($y :$ $l = 3 : 5$).	32
2.16 Typical static force operated by the actuator in function of the contraction ratio and comparison of three various size of the actuator in typical pres- sure(34.5kPa).	33
2.17 Fabrication process to include integrated electronics in the actuator.	35

2.18 The experimental plot to compare with between distance of the outer actuator and displacement of the inner actuator, (a) The relationship between the inner actuator and voltage, (b) The relationship between the inner actuator and the outer actuator, (c) The relationship between the outer actuator and voltage.	39
2.19 The cycling test of the actuator including the integrated electronics.	40
3.1 (a) A novel soft pneumatic exoskeleton for elbow joint in the initial state. (b) A novel soft pneumatic exoskeleton for elbow joint when it is inflated.	42
3.2 Two support structures of the exoskeleton. .	43
3.3 The main actuated region of the exoskeleton. .	43
3.4 All parts of the exoskeleton. .	44
3.5 A manufacturing process for the arm exoskeleton based on the manufacturing system of the submitted paper. .	45
3.6 Photos of the exoskeleton on an arm demonstrating the range of motion. . .	46
3.7 Additional photos of the exoskeleton on an arm. .	47

Chapter 1

Introduction

Robotic systems are becoming increasingly prevalent today, with possible applications including personal or mobile robots working alongside humans and exoskeletons worn to restore or improve human abilities. There are many types of robots such as industrial robots [10], socially assistive robots [11], and biomimetic robots [12]. Additionally, exoskeletons [1–3] attempt to overcome bodily disabilities and maximize their wearers' performance.

Most exoskeletons were invented to facilitate human-robot interaction. Regarding the interaction between robots and human motion, biology has long been a source of inspiration for researchers making more capable machines.



Figure 1.1: An exoskeleton robot for assisting rehabilitation of arm functions [1].



Figure 1.2: A Self-Contained Transfemoral prosthesis leg [2].



Figure 1.3: University of California at Berkeley’s BLEEX exoskeleton [3].

Within robot technology research, the soft robotics field is developing rapidly and is poised to have a wide impact in a variety of applications. Soft robots have intrinsic compliance, offering a number of benefits as compared to traditional rigid robots. Compliance can provide compatibility with biological systems such as the human body and can provide some benefits for human safety and control. Further research into soft robots can be advanced by further development of pneumatic actuators. Traditional rigid robots are widely used in manufacturing systems and can be specifically programmed to perform a single task efficiently, but they have limited adaptability. This is because these robots can be heavy and

bulky, and they are designed with rigid links, actuators and joints. Of course, conventional robots can be controlled, designed and simulated with various programs to minimize the risk to humans and perform various tasks, but drawbacks remain. In contrast to these traditional robots, soft robots are usually made of soft and extensible materials such as silicone, rubber, and fabric, which is intrinsically compliant. Because of these properties, these soft materials have the great advantage of being able to absorb energy during a collision preventing injury. Moreover, the soft materials can provide natural human-robot interaction, although their control is more difficult than with traditional rigid robots. Therefore, research into soft robotics is worth pursuing.

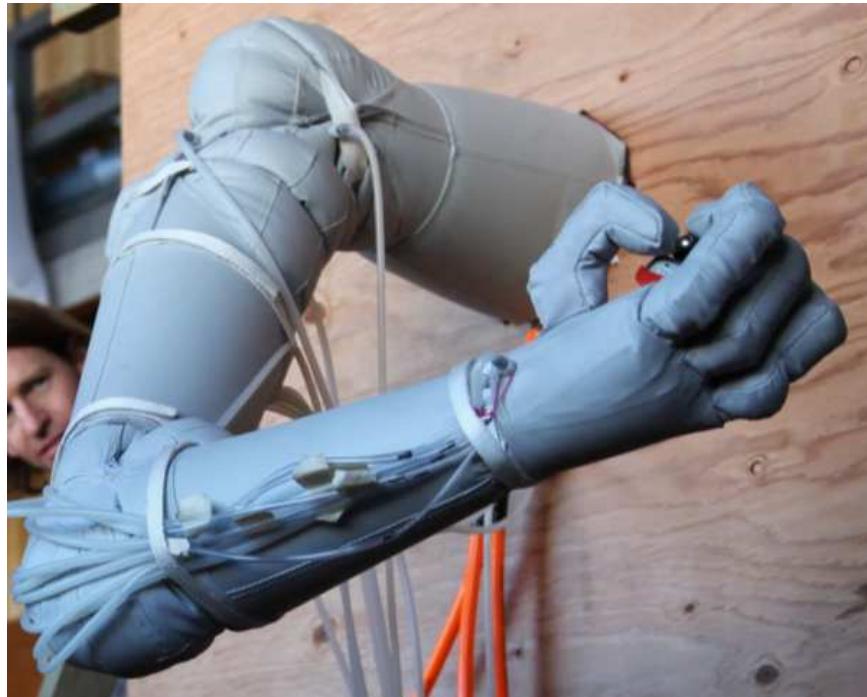


Figure 1.4: Pneumatic robotic arm made from textiles [4].



Figure 1.5: A pneumatic arm exoskeleton made by Otherlab [5].

In the soft robotics field, while there are a variety of possible actuation schemes, pneumatic actuators present some benefits as they can be very light-weight, compact, and use flexible materials. With these benefits, various types of soft actuators have been introduced. In this paper, we will present our novel pneumatic actuator, which is built completely of fabric based on the process in Chapter 2, and a new type of soft exoskeleton in Chapter 3. The soft exoskeleton is for the elbow joint, which in the future could help people hold heavy weights, and could serve in the rehabilitation of certain injuries.

Chapter 2

Modeling and Analysis of a novel pneumatic artificial muscle

2.1 Abstract

We present a novel pneumatic artificial muscle made of textiles or plastics with integrated electronics to sense its pressure and displacement. Compared to traditional pneumatic muscle actuators such as the McKibben actuator and other more recent soft actuators, the actuator described in this paper can produce a much higher (40-60%) contraction ratio. In this paper, we describe the design, fabrication, and evaluation of the actuator, as well as the manufacturing process used to create it. We demonstrate the actuator design with two examples that produce 120N and 300N at pressures of 35 kPa and 105 kPa, respectively, and

have contraction ratios of 40% to 65%.

2.2 Introduction

Robotic systems are becoming increasingly prevalent today, with possible applications including personal or mobile robots working alongside humans [13–15] and exoskeletons worn to restore or improve human abilities [16–19]. While there are a variety of possible actuation schemes, pneumatic artificial muscles present some benefits as they can be very light-weight, compact, and use flexible materials. They can also be intrinsically compliant, providing natural human-robot interaction or increasing safety in the event of human-robot collisions. With these benefits, a number of groups have investigated different pneumatic actuator geometries and fabrication methods.

In the following paragraphs, we review the state of the art in pneumatic actuators. We provide a classification framework for the different types of actuators, which illuminates opportunities for new types of actuators. Figure 2.1 presents this classification framework and shows illustrations of the different types of pneumatic actuators described in the literature as well as the actuator developed in this paper.

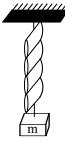
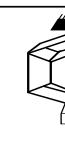
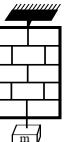
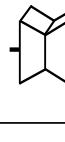
Class I : Contraction with positive pressure			
	Operation Principle		Max. Contraction Ratio
	Initial State	Final State	
Peano muscle / Flat PAM			15%
McKibben Muscle / PPAM			35%
Our Actuator			65%
Our Actuator			50%
Class II : Contraction with vacuum			
VAMPs			30%
Bellows textile muscle			89%
Class III : Expansion with positive pressure			Max. Expansion Ratio
	Initial State	Final State	
Fast Pneu-nets Actuator			65%
Our Inner Actuator			900%

Figure 2.1: A classification framework for the different types of actuators, Class I : Peano muscle / Flat PAM, McKibben Muscle / PPAM and Our Actuator, Class II: VAMPs and Bellows textile muscle, Class III: Fast Pneu-nets actuator and our inner actuator.

The first class of pneumatic actuators is those that contract when positive pressure is applied. The most well-known example of these is the McKibben actuator [20]. The McKibben actuator has a structure consisting of an inner rubber tube with a mesh sleeve covering the tube. When the inner tube is pressurized, the mesh sleeve causes the structure to shorten; the specific shape is dictated by the mesh weave angle [21]. Many researchers have analyzed the McKibben actuators properties, including the design, contraction velocity, contraction ratio, and operating force over a range of pressures [22, 23]. For this paper, we define an actuator's contraction ratio as:

$$CR(\%) = \left(1 - \frac{k_0 - \Delta k}{k_0}\right) \times 100 \quad (2.1)$$

where k_0 is the initial length of the actuator and Δk is the length it shortens during contraction.

However, the general McKibben actuator has some drawbacks: it has a low contraction ratio (30-35%) because of the geometry and the dead volume inside the actuator when uninflated, it exhibits friction between the mesh and inner tube that can lead to failures, and it requires deformation of the inner tube which can lead to fatigue and lower controllability at low pressures.



Figure 2.2: The McKibben actuator.

To solve the problems of friction and deformation of the inner tube, Braided pneumatic artificial muscles [23–26] and Pleated Pneumatic Artificial Muscles (PPAM) [27–29] have been developed for many applications such as a biped robot [30], a lower-body exoskeleton [31,32] and an arm exoskeleton [33]. Their outer structures are different from the traditional McKibben muscle in that they are made of a single layer of aromatic polyamides, which eliminates friction between the layers. These material properties give the PPAM increased performance and accuracy compared to the McKibben muscle, with a similar contraction ratio.



Figure 2.3: Pleated pneumatic artificial muscles(PPAM).

Another type of soft actuator is a Peano-fluidic muscle [34] which is made of materials such as fabric or PVC film. Its structure consists of a few layers that lie flat in their initial state and are bonded at intervals in lines perpendicularly to the contraction direction. When air pressure is applied, the flat shape inflates to become round, causing the length of each of the tube segments to contract into its final state. This technology has been used as a soft leg exoskeleton [35] and as a rotational actuator [36,37] and has a contraction ratio of 15%.

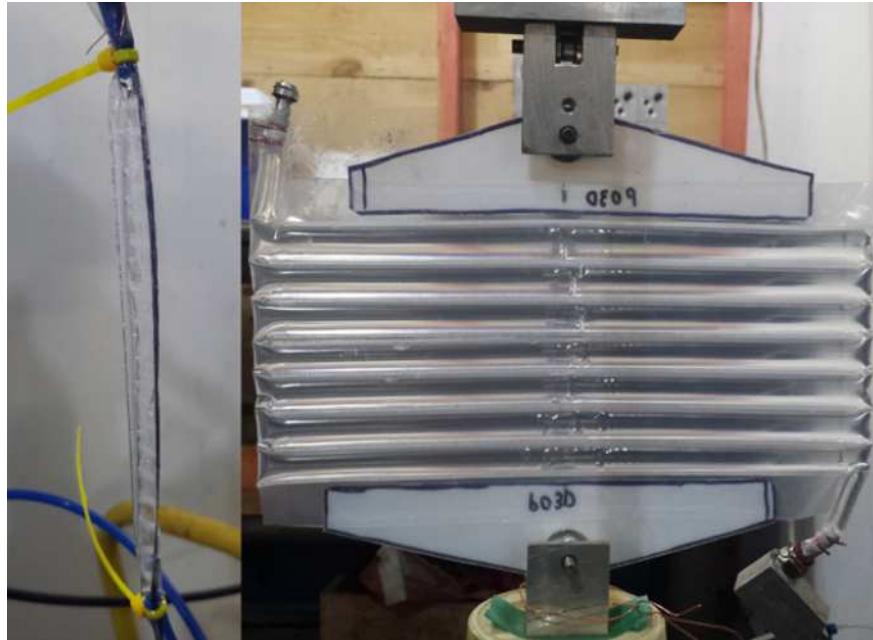


Figure 2.4: A peano-fluidic muscle.

In each of these cases, the contraction ratio is relatively small because an initial shape that is relatively tall and thin is expanded to be more spherical or cylindrical; inextensible fibers convert this expansion in the lateral direction to a contraction in the lengthwise direction. This behavior combined with the fixed device circumference provides a fundamental limit on the contraction ratio. In the limit, in two dimensions a very tall and narrow rectangle with height k will expand at most to a circle with height ($2\pi k = 0.636k$, corresponding to a contraction ratio of 36.4% (Figure 2.5(a)).

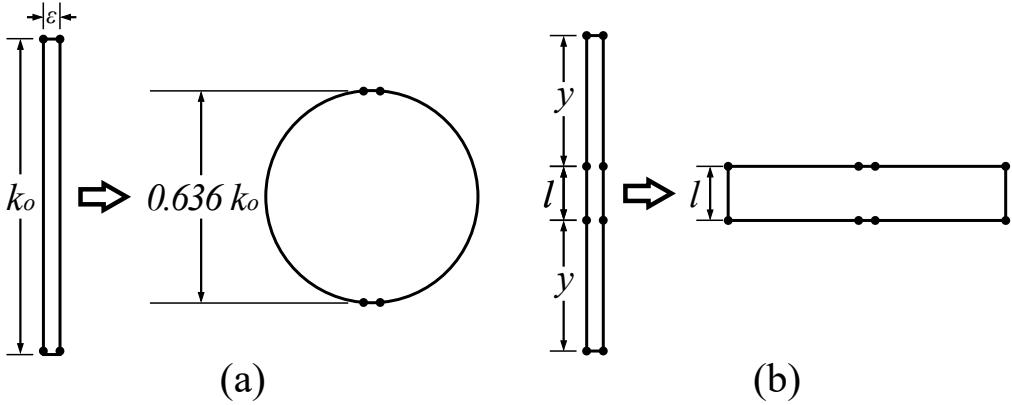


Figure 2.5: A schematic figure of the operating principle of mechanisms that contract when expanded horizontally, assuming a constant edge length. (a) Traditional pneumatic actuators start out tall and thin and contract to become more cylindrical or spherical. (b) Greater changes in length can be achieved if the final state can be a wide rectangle instead of a circle. The pneumatic actuator developed in this paper uses this structure.

The second class of actuators in our framework includes those that contract when negative pressure (vacuum) is applied. In contrast to the actuators in the first class, there is no fundamental physical limit on the lengthwise contraction for a given actuator length. One example of this type is a Bellows textile muscle [6], similar to the Peano fluidic muscle. The actuator is made of fabric and is constructed by connecting a number of round discs along their edges and centers. Since the actuator is made of textiles, it collapses to be extremely flat, giving it a contraction ratio of 89%. While not designed for this purpose, if used in expansion this would correspond to an expansion of up to 900% of its initial length.



Figure 2.6: A Bellows textile muscle [6].

Another example of this class is the Vacuum-Actuated Muscle-inspired Pneumatic structures (VAMPs), which is a buckling pneumatic linear actuator [7]. The actuator has a complex structure that includes vertical beams, horizontal beams, and collapsible air chambers. When vacuum is applied, collapsed air chambers cause the horizontal beams to buckle, resulting in a large length change in vertical direction. Since this actuator is made from silicone rubber, it cannot collapse as compactly as the Bellows textile muscle, giving it a contraction ratio of 30%.

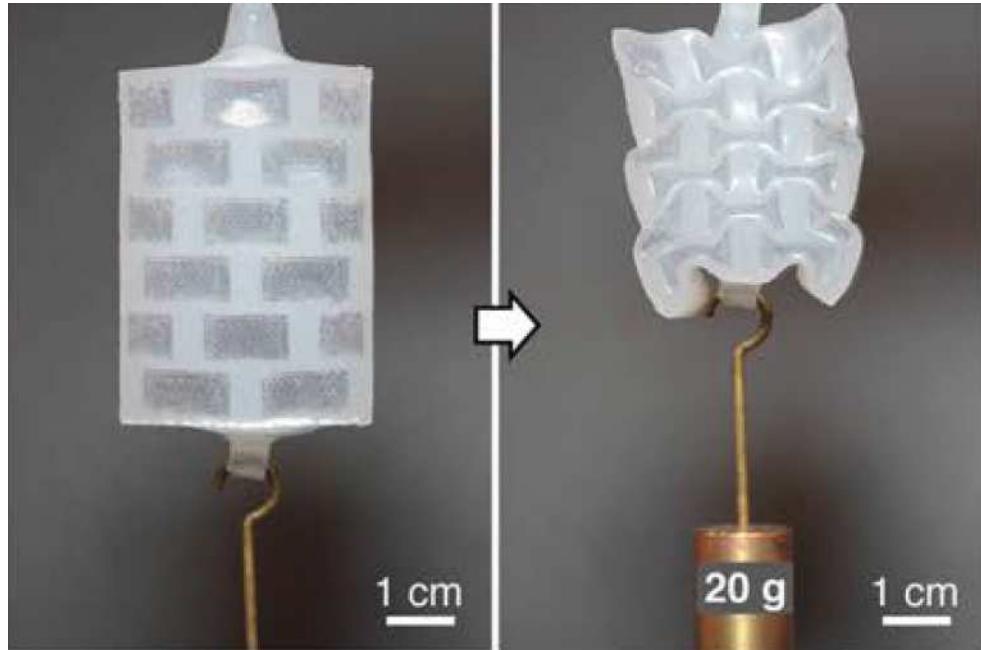


Figure 2.7: Vacuum-Actuated Muscle-inspired Pneumatic structures (VAMPs) [7].

While the actuators in this class can achieve impressive contraction ratios, they are fundamentally limited in the amount of force they can generate for a given actuator cross-section due to their use of negative pressure. Actuators powered by positive air pressure can potentially achieve extremely high pressures, but actuators depending on vacuum are limited to atmospheric pressure.

The third class of actuators is those that expand under positive pressure. An example of this type is the Fast Pneu-Nets actuator (fPN) [8, 9], which is fabricated with a silicone elastomer. The actuators structure is divided by two parts: a top layer that expands and an inextensible layer on the bottom. When positive air pressure is applied, flat chambers in top layer inflate to become round, pushing on adjacent chambers and causing the structure

to curl in conjunction with the inextensible layer.

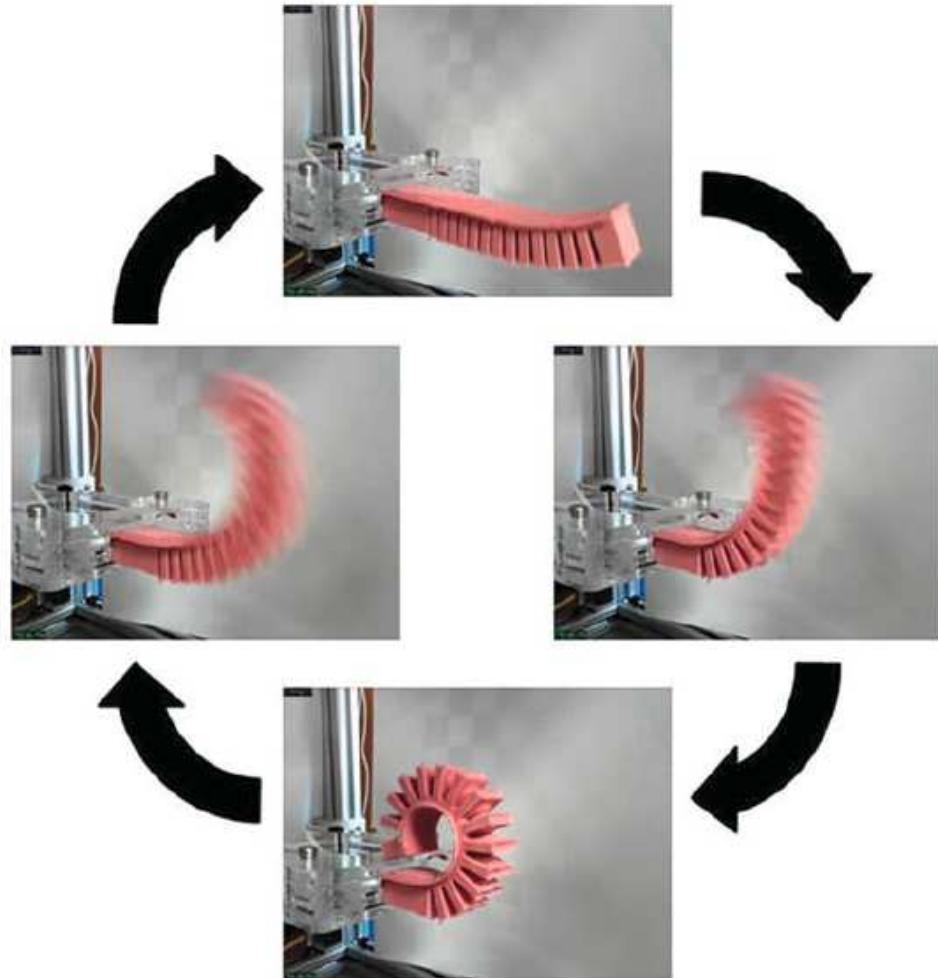


Figure 2.8: The Fast Pneu-Nets actuator (fPN) [8, 9].

A possible fourth class of actuators is those that would expand when provided with negative pressure (vacuum), although we did not find any examples of this in the literature, presumably because the benefits of such an actuator would not be significant. An example of a structure that would accomplish this behavior is a spherical structure that collapses to

a cylinder when actuated; such a structure would likely need to be relatively rigid to enforce the desired geometric transformation.

It is also interesting to note that the actuators discussed previously were either made from thin sheets of textile or plastic, or were molded out of silicone or other polymers. Many of the structures can be made from either method. While many very clever geometries can be fabricated out of silicone or other polymers, molded actuators do have some drawbacks. Their fabrication process is complex, and since the material is required to stretch during the actuators' operation, there is the potential for the material to fatigue and rupture over time if not designed properly [38]. However, molded actuators have many benefits as well including permitting structures to move through a mechanically-programmed motion profile [39, 40].

In summary, the pneumatic actuators in each of the four classes have different strengths and limitations. The actuators in Class I to date can have a high force densities, but suffer from relatively small contraction ratios. In Classes II, the force density is limited by atmospheric pressure, although large contraction ratios are possible. Actuators in Class III have been limited to those that can bend instead of extend linearly.

This paper presents a novel pneumatic actuator that overcomes many of the shortcomings of prior work. In particular, the actuator can achieve very high contraction ratios (40-60%) through the mechanism roughly illustrated in Figure 2.5(b). By creating an actuator structure that forms a wide rectangle instead of a sphere (in two dimensions) when expanded, much higher contraction ratios can be achieved. Additional advantages are that it collapses to be flat; it does not have friction between an outer actuator and inner actuator that may

decrease its lifetime; it has a simple manufacturing process; and it can include integrated electronic sensors. The latter is possible because the actuator is constructed from a textile or plastic sheet and is designed so the material bends but does not stretch during operation. The remainder of this paper is organized as follows. We introduce the concept of the pneumatic actuator and its geometry in Section 2. We then discuss the fabrication process in Section 3, show a mathematical model of the actuator in Section 4, and present results of experiments characterizing the performance of the actuator in Section 5.1. Finally, in Section 5.2, we present the fabrication process for modifying the actuator to include integrated electronics for controlling and monitoring displacement and pressure in real time.

2.3 Overview

The pneumatic actuator described in this paper is shown in Figure 2.9. It consists of an “inner actuator” formed by a series of connected chambers, and an “outer actuator” composed of two additional pieces of material (Figure 2.9(e) and 2.9(f), respectively). In the initial state with no air pressure, the actuator is flat (Figure 2.9(a)), and the structure creates no force. When positive air pressure is applied to the inner actuator, the inner actuators inflate and expand horizontally. The outer actuator then converts the horizontal motion of the inner actuators to a motion that contracts the actuator vertically (Figure 2.9(b)). The resulting structure is similar in geometry to a linkage used with piezoelectric energy harvesters to maximize their force [41, 42]. The overall scheme of the actuator is illustrated in Figure

2.9(b). If a structure that is initially thin and flat expands into a rectangular structure, it can achieve a very high contraction ratio. Our actuator and the inner actuator as a standalone device are also shown in Figure 2.1, in Classes I and III respectively.

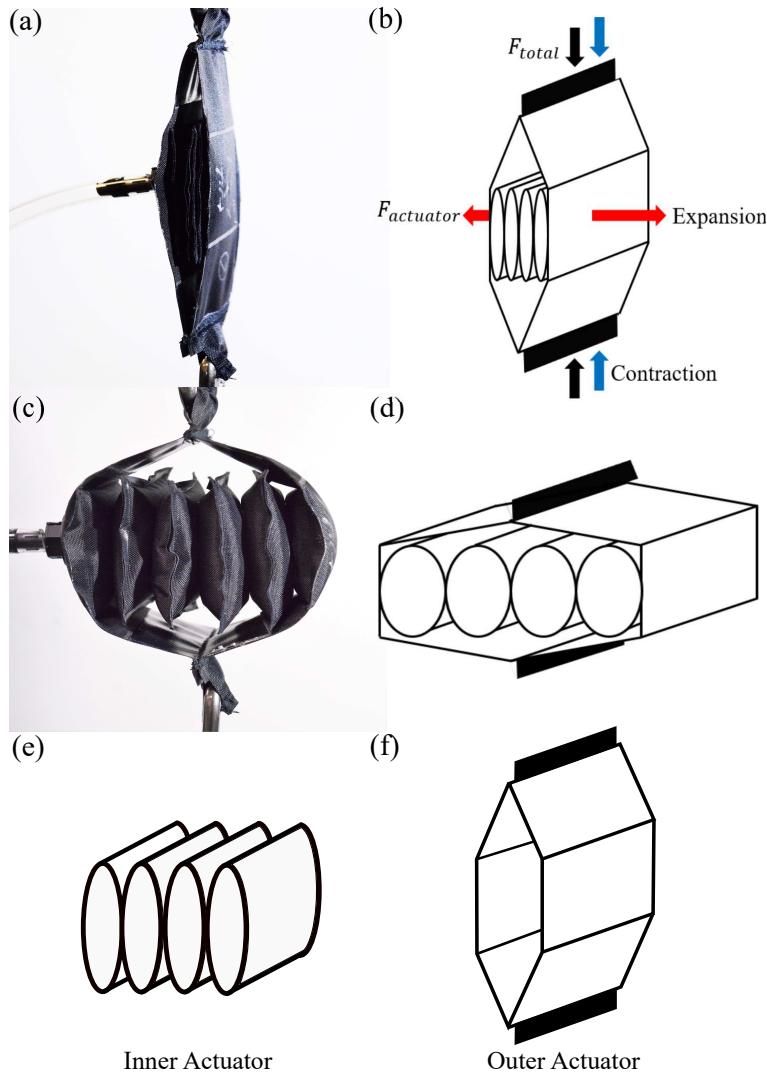


Figure 2.9: The concept of the actuator: (a) Initial state of actuator prototype, (b) Initial state of actuator model, (c) Final state of actuator prototype, (d) Final state of actuator model, (e) Inner actuators, (f) Outer actuators.

The actuator can be made from thin plastic sheeting or from a textile coated with rubber or plastic so that it is airtight. A key feature of the actuator is that it does not require the material to stretch during its operation, a property it shares with other textile actuators such as the Peano fluidic muscle and the Bellows textile muscle. With this behavior, rigid or semi-rigid structures can be easily integrated with soft structures by simply affixing them to the material. Since the material does not stretch, the elastic modulus is similar to that of the rigid or semi-rigid materials, minimizing stress concentrations at the junction. We use this behavior to attach rigid electronic circuit boards to the actuator. In contrast, a structure made from a material like silicone that undergoes significant stretching will generate high stress concentrations at the interface with a rigid or semi-rigid material and require intervening material with an intermediate stiffness [43].

We present a version of the actuator that includes integrated electronics in Figure 2.10. The actuator has the same assembly process with the addition of two thin plastic structures, one at each end of the inner actuator. One plastic structure includes an LED board at the center, and the other includes a pressure sensor and an ambient light sensor to measure displacement in conjunction with the LED. These sensors provide information about the state of the actuator.

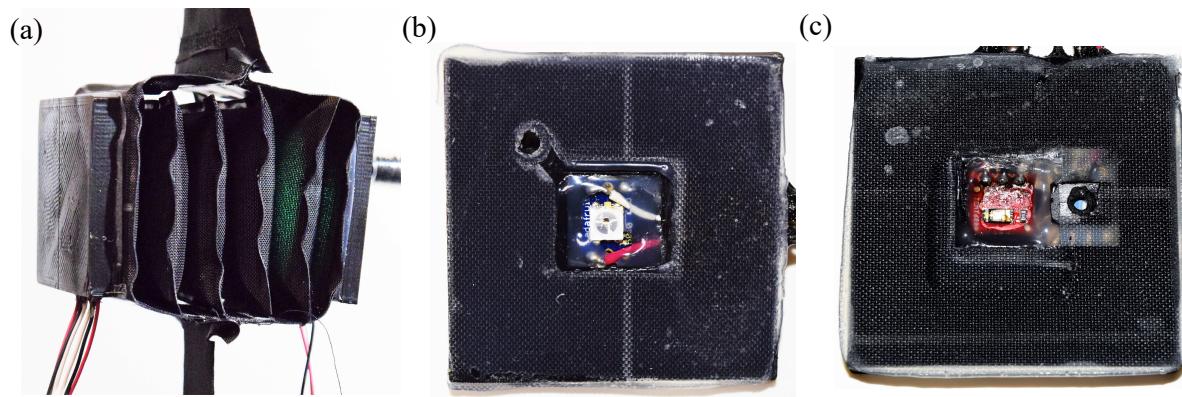


Figure 2.10: The concept of the actuator including integrated electronics (a) Actuator prototype, (b) The first thin plastic structure embedding an LED board, (c) The second plastic structure attaching a displacement sensor and a pressure sensor.

2.4 Materials and Methods

2.4.1 Fabrication Methods

We developed a quick and simple fabrication process for the actuator (Figure 2.11) which was made of heat sealable oxford fabric with a urethane film coating on one side (Heat Sealable Oxford, 200 Denier, Seattle Fabrics, Inc.), along with a thermal adhesive film (Fastelfilm 20093, Fastel Adhesive and Substrate Products, Inc.). The manufacturing process is separated into two parts: (1) bonding the inner edges in the actuator using a thermal adhesive film, and (2) bonding the outer edges on the actuator using a heat sealer. The fabrication process is divided into two parts because the fabric is only coated with the Urethane film on one side; the uncoated side can only be bonded with the thermal adhesive film, while the coated side can only be bonded with the heat sealer.

In the first part, shown in Figure 2.11 steps 1 and 2, the fabric sheets and thermal adhesive film layers are prepared according to the size of the inner connection parts and the number of inner layers. After the fabric and thermal film layers are cut, they are aligned, clamped together, and put in an oven at $250^{\circ}F$ for 10 minutes.

The second part of the fabrication process includes steps 3-5 in Figure 2.11. In step 3, the outer edges of each pouch in the inner actuator are bonded using a heat sealer. In steps 4 and 5, the outer actuator is bonded to the inner actuator and completed using the heat sealer.

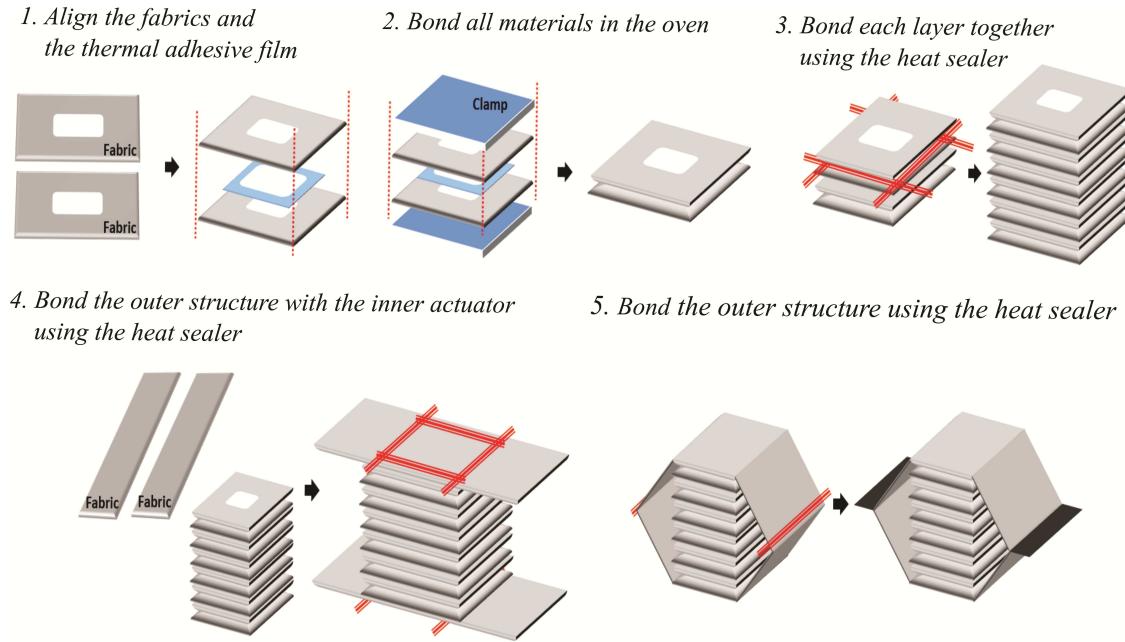


Figure 2.11: The manufacturing process of the actuator: Steps 1, 2, and 3 are for the fabrication of the inner actuator, and steps 4, and 5 are for the fabrication of the outer actuator.

2.4.2 Actuator Modeling

We next present a mathematical model of the actuator (Figure 2.12), which includes separate portions for the outer and inner actuators (Figure 2.12(a) and 2.12(b) respectively). We use the model to design an actuator with a desired peak actuation force F_{total} of 120N at 34.5kPa and 300N at 105kPa, and a contraction ratio of over 60% in order to overcome the disadvantages of other actuators.

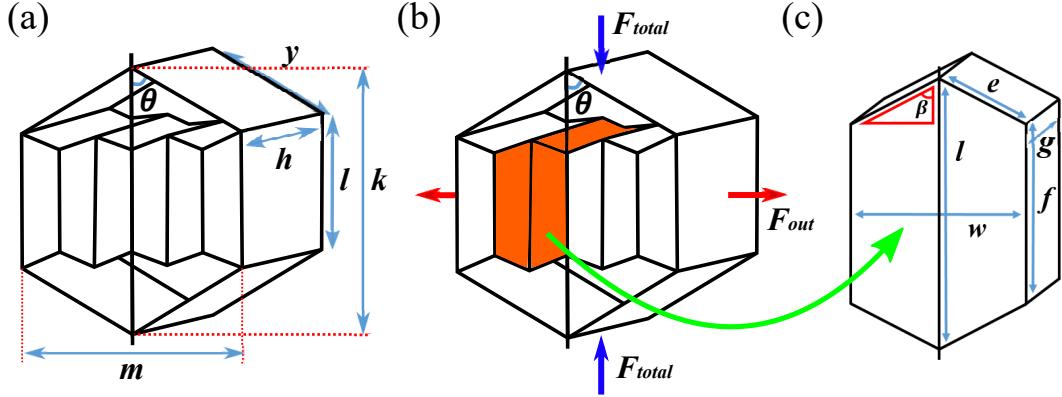


Figure 2.12: The mathematical models of the actuator, (a) The diagram of the actuator, (b) The inner structure of the actuator, and (c) A single unit of the inner actuator.

Outer Actuator Modeling

We first model the outer actuator, with the diagram and variables in Figure 2.12(a). The inner actuator pushes on the middle portion of the outer actuator over a rectangular cross section, with a total outward force (F_{out}), where

$$F_{out} = P \times h \times l \quad (2.2)$$

and P is the pressure inside the inner actuator, h is the width of the inner and outer actuators, and l is the height of the rectangle where the inner actuator connects to the outer actuator. The structure of the outer actuator (Figure 2.12(b)) leads to the following relationship between total contractile force from the outer actuator (F_{total}) and the outward force from the inner actuator (F_{out}):

$$F_{total} = \frac{1}{2} \times F_{out} \times \tan^{-1}\theta \quad (2.3)$$

where θ is the angle between vertical and either of the top links in the outer actuator. We can calculate how much force the actuator will supply using Equations 2.2 and 2.3 to obtain the following expression:

$$F_{total} = \frac{1}{2} \times P \times h \times l \times \tan^{-1}\theta \quad (2.4)$$

Equation 2.4 is used to choose the outer actuator geometry.

As shown in Figures 2.5(b) and 2.12(a), the contraction ratio of the actuator is dictated by the ratio between the height of the inner actuator (l) and the length of the outer actuator between the top and the inner actuator (y). The initial actuator length is then $k_0 = 2y + l$; when the actuator is fully contracted, the new length $k = 2y \cos(\theta) + l$ is then approximately l , for a change in length of approximately $\Delta k = 2y$. The contraction ratio can then be computed by plugging Δk and k_0 into Equation 2.1. With reasonable choices for y and l , it is possible to achieve contraction ratios between 40% and 70%.

Inner Actuator Modeling

Given the geometry of the outer actuator, we next describe how to design the inner actuator, including both the geometry and number of layers. We first model the inner actuator as a

series of chambers connected together at their ends; Figure 2.12(b) shows one chamber in the inner actuator highlighted in orange, and Figure 2.12(c) shows a close view of the chamber. We model the chamber as a geometric solid with straight edges, although in reality the chamber will have complex three-dimensional curves. In this simplified model, the short edges of the chamber are of length f and width g , the distance between the center connections and the edge is e , and the distance across the chamber is w . The actuator's maximum volume can be calculated using lengths w , e , and f . The volume of the single unit of the inner actuator is:

$$V = \frac{4}{3}w(e^2 - (\frac{w}{2})^2) + wfg + w(f+g)\sqrt{(e^2 - (\frac{w}{2})^2)} \quad (2.5)$$

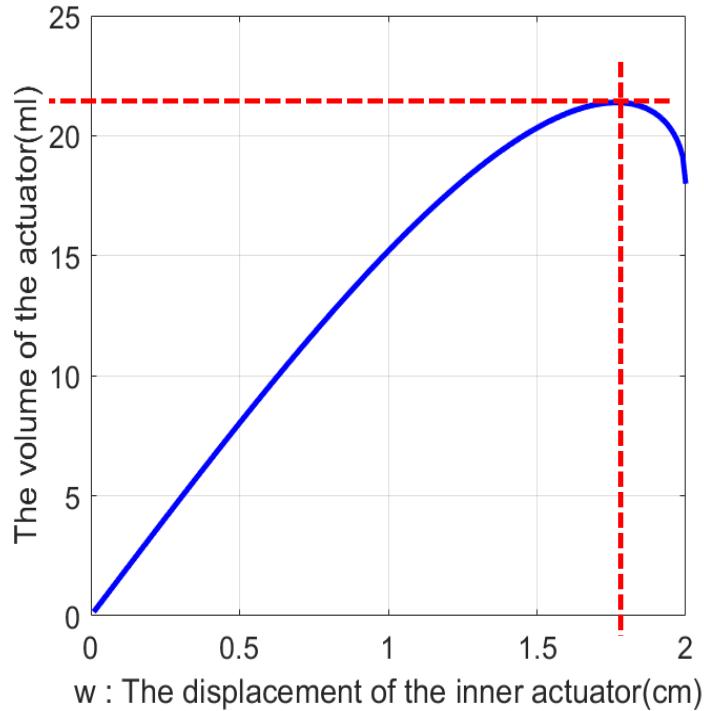


Figure 2.13: Simulation of the volume versus displacement of a single chamber in the inner actuator using the model in Figure 2.5, for sample lengths of $y=4\text{cm}$, $f=3\text{cm}$, $g=3\text{cm}$ and $e=1\text{cm}$.

which is also shown in Figure 2.13 for sample lengths of $y=4\text{cm}$, $f=3\text{cm}$, $g=3\text{cm}$ and $e=1\text{cm}$. The maximum volume inside the actuator as a function of the variables in Equation 7 cannot in general be found analytically, but it and the corresponding maximum width $w_{max}=1.77\text{cm}$ can be found numerically. The maximum width gives the maximum amount each chamber in the inner actuator will expand during operation. Thus, to enable the outer actuator to have its maximum range of motion, there must be at least N inner actuators, where

$$N = \text{ceil} \left(\frac{2y}{w_{max}} \right) = \text{ceil} \left(\frac{6}{1.77} \right) = \text{ceil} (3.38) = 4 \quad (2.6)$$

2.5 Results and Discussion

2.5.1 Experimental Evaluation

We fabricated a variety of actuators with different geometries to characterize their performance. For our test actuators, we selected $h=5\text{cm}$ and $l=5\text{cm}$ to make the actuators relatively compact. We then selected $y=4\text{cm}$ to obtain a contraction ratio around 60%. This geometry provides a contraction force F_{total} of 120N at 34.5kPa, 300N at 105kPa.

For our test actuator, we selected length (f) to be 3cm. From Equation 2.6, we see that this test actuator needs over 5 inner actuators to obtain the full range of motion.

In experiment 1, we fabricated two actuators with the same total length k_0 and different ratios between y and l . Both actuators had a width chosen so the inner actuator was square in cross-section, so $l=w$ and $f=g$

The test actuator was fabricated with the dimensions and processes detailed above, then analyzed to understand its performance. In the first experiment, an Instron 4204 machine was used to characterize its low-frequency motion and properties. Two actuators with equal total length (k) but different dimensions for

extity and l were prepared to test the behavior with varying geometry (Figure 2.14). The

first and second actuator dimensions used for the test were $y=4\text{cm}$, $l=5\text{cm}$, $h=5\text{cm}$, and $f=3.3\text{cm}$; and $y=3\text{cm}$, $l=7\text{cm}$, $h=7\text{cm}$, and $f=5\text{cm}$, respectively. The experiment, in Figures 2.14(a) and 2.14(b), shows the force produced by each actuator at 34.5kPa and 69kPa. The total length of each actuator is 13cm, but there is a difference in contraction ratio due to the different lengths (y). The first and second actuators have contraction ratios of approximately 60% and 40% at 34.5kPa with forces up to 160N and 180N respectively. The difference in peak force is because the second actuator has a bigger inner structure. With 69kPa, two actuators generate approximately 1.8~2.0 times more force than those at 34.5kPa with a slight increase in contraction ratios because the fabric does stretch slightly (1~2%) under high tensile forces.

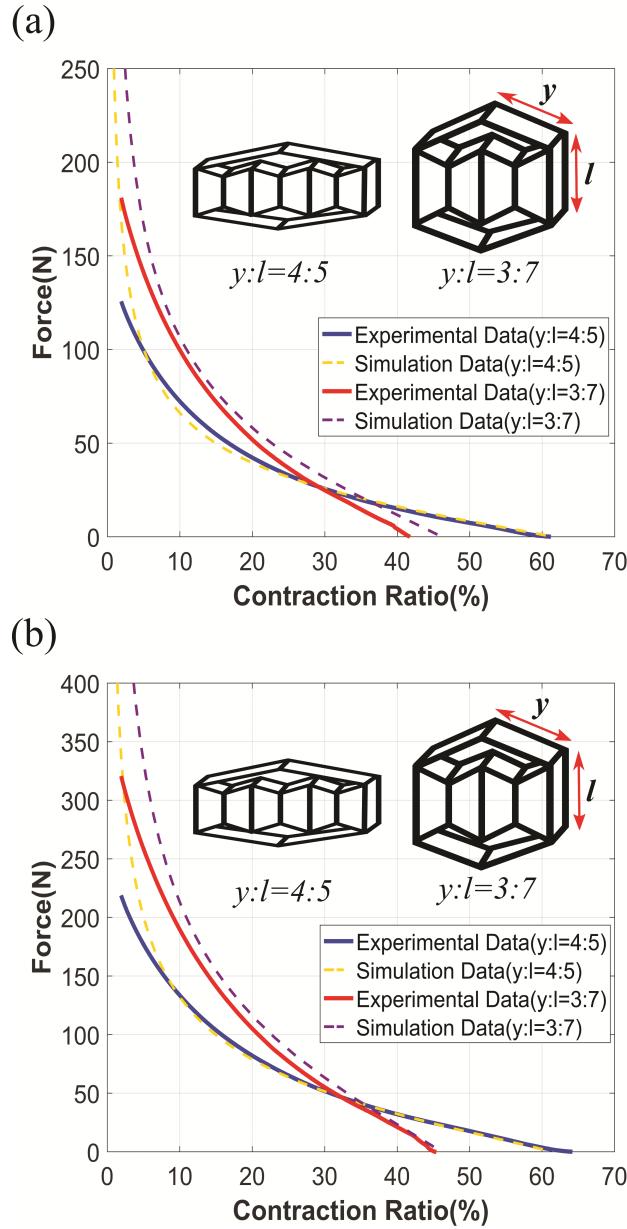


Figure 2.14: Typical static force operated by the actuator in function of the contraction ratio and comparison between two various size of the actuator (a) The property at typical pressure (34.5kPa) (b) The property at typical pressure (69kPa).

The second experiment tests each actuator under various conditions (34.5~103.5kPa). In

Figure 2.15(a), an actuator with $y=2\text{cm}$, $l=5\text{cm}$, $h=5\text{cm}$, and $f=3.3\text{cm}$ is prepared. Depending on the pressure, the actuator can make up to 125N force at 34.5kPa, and generate approximately 1.8~2.0 times more force whenever twice the amount of pressure is applied. As expected, its contraction ratio only changes slightly as the pressure is varied from 34.5kPa to 103.5kPa. In Figure 2.15(b), we used an actuator with $y=3\text{cm}$, $l=5\text{cm}$, $h=5\text{cm}$, and $f=3.3\text{cm}$. According to the simulation data, the actuator in Figure 2.15(b) generates the same amount of force as the actuator in Figure 2.15(a) because the size of their inner actuators are the same. However, the peak force differs by 10-20N due to imperfections in fabrication. Comparing Figures 2.15(a) and 2.15(b), there is a 10% difference in contraction ratios because of differing lengths (y). From the data, the novel pneumatic actuator can be competitive with the traditional McKibben actuator.

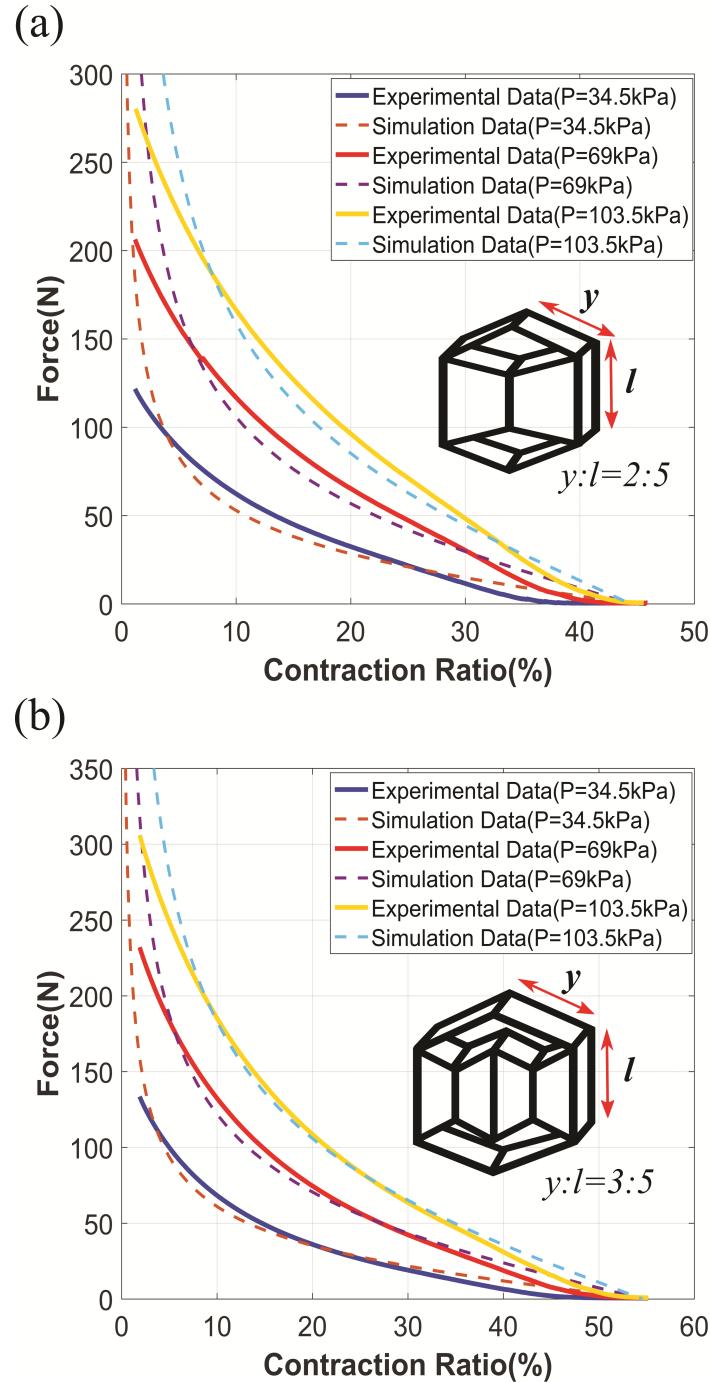


Figure 2.15: Typical static force operated by the actuator in function of the contraction ratio and comparison the force regarding various pressure ranges (a) The property of the actuator($y : l = 2 : 5$) (b) The property of the actuator($y : l = 3 : 5$).

The next experiment compares the properties of each actuator at the same pressure conditions. According to the actuator model, every actuator with the same inner actuator cross section generates the same peak total force (F_{total}) with differing contraction ratios due to different lengths (y). Figure 2.16 shows the force versus contraction ratio for several actuators with different lengths (y). The plot shows that indeed they can generate the same peak force, neglecting a 5~10N error due to variations in fabrication.

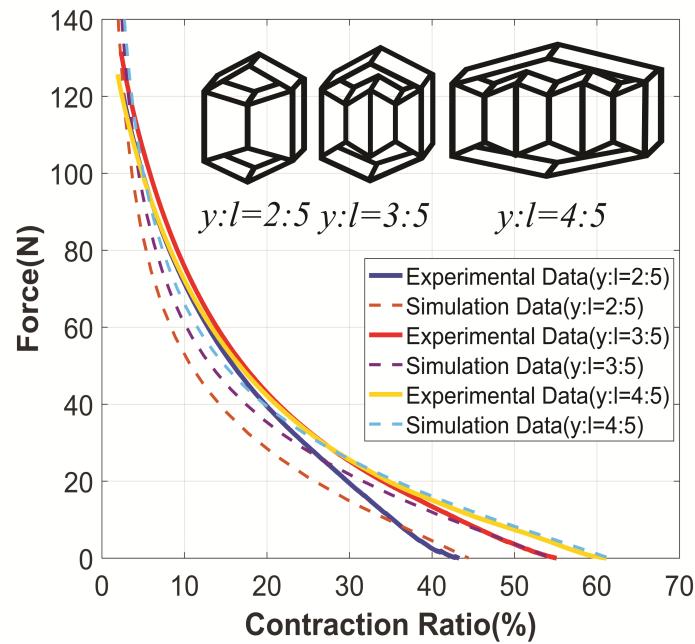


Figure 2.16: Typical static force operated by the actuator in function of the contraction ratio and comparison of three various size of the actuator in typical pressure(34.5kPa).

2.5.2 Electronics Integration and Evaluation

In order to use the novel actuator as a core component of a robot, the force and/or length of the actuator must be sensed. Instead of using external sensors, we accomplish this by embedding electronics within the actuator itself. Specifically, we sense the displacement by using an ambient light sensor and light emitting diode (LED) at opposite ends of the inner actuator. We also sense the pressure inside the inner actuator with a pressure sensor, which can be converted to force by knowing the outer actuator's geometry.

To incorporate electronics, the fabrication process is modified slightly with additional steps to add the electronics as shown in Figure 2.17. First, we 3-D printed two ABS plastic parts to serve as substrates for the electronics on each end of the inner actuator. We then embedded the LED in the center of one piece, and the ambient light sensor and pressure sensor in the center of the other. In each side, the wires protrude through a hole in the back of the plastic part. To seal this hole and prevent air leaks, we next poured liquid ABS, made by mixing Acetone and ABS material, into the hole around the wires, and waited for the liquid ABS to fully cure, around 24 hours. Finally, we attached the plastic parts to the actuator using the thermal adhesive film.

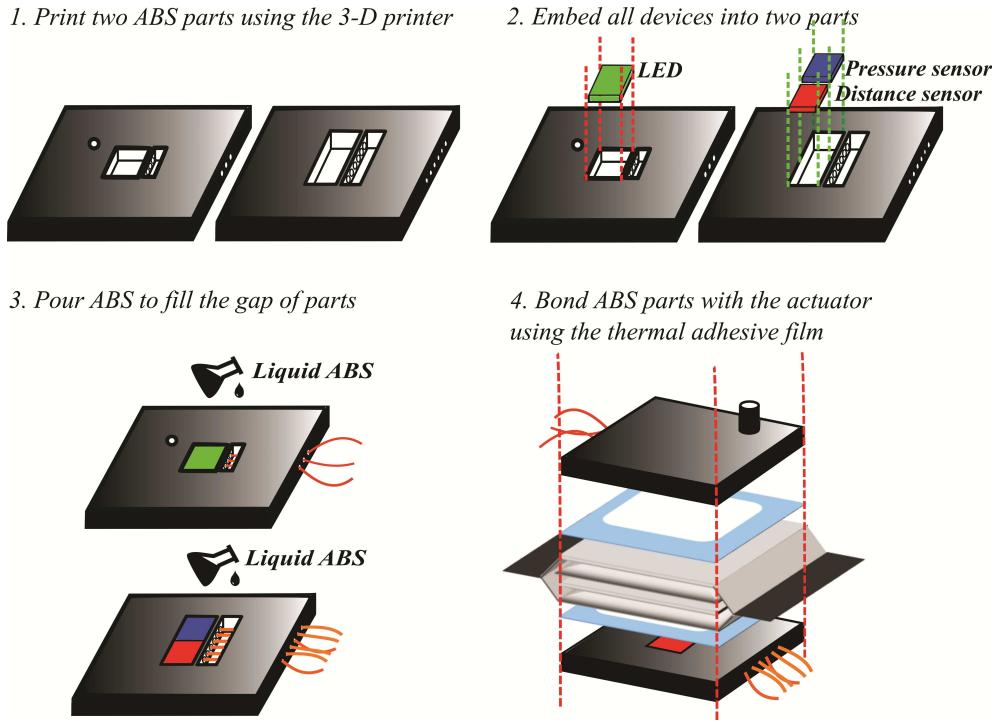


Figure 2.17: Fabrication process to include integrated electronics in the actuator.

We tested the sensorized actuator to determine the relationship between the distance of the outer actuator (k) and the displacement of the inner actuators (m), which could be used to precisely control the actuator. We determined this relationship using an Instron machine with an actuator geometry of $y=3\text{cm}$, $l=5\text{cm}$, and $h=5\text{cm}$. During the tests we maintained a constant actuator pressure of 69kPa while the Instron machine varied the actuator length.

Figure 2.18(a) shows the relationship between voltage (V) and the inner actuator length (m). To create this graph, the Instron machine was used to control the inner actuator length while the voltage output from the sensors was measured. Since the electronics are composed of an LED shining on a photodiode, the amount of light falling on the photodiode will vary

as:

$$m = a\sqrt{\frac{1}{V}} + b \quad (2.7)$$

Where m is the displacement of the inner actuator and V is the voltage output. Since it is very difficult to estimate the cross-sectional area of the photodiode that will be sensitive to incoming light, we fit the measured curve to this form. The resulting best-fit line was:

$$m = 2.64\sqrt{\frac{1}{V}} - 0.126 \quad (2.8)$$

Figure 2.18(b) shows the modeled and experimental relationship between the inner actuator distance and the outer actuator distance. For the plot, we tested the outer actuator length using the Instron machine and the inner actuator length using integrated electronics at the same time.

In the Figure, the displacement of the inner actuator was calculated by the Equation 2.8 with measuring the resulting voltage, and the outer actuator distance was measured by Instron machine. There is an offset of the inner actuator distance of 1cm because the electronics prevent the actuator from lying completely flat. In the plot, it can also be seen that the maximum inner actuator displacement is 6cm, which follows from the geometry of the actuator.

We used the geometry of the actuator in combination with equation to generate the “Theo-

retical” curve in Figure 2.18(b), while the “Experimental” curve was measured on the Instron machine. The Theoretical curve thus has the equation:

$$k = l + 2\sqrt{y^2 - \frac{m^2}{4}} \quad (2.9)$$

Where k is the length of the outer actuator, l is the height of the rectangle, and y is the length of the outer actuator between the top and the inner actuator as shown in Figure 2.12(a).

In figure 2.18(c), we plot the sensor output voltage (V) versus the outer actuator length (k). These data were collected by moving the outer actuator with the Instron machine and measuring the resulting voltage. The figure shows the experimentally-collected data as well as the “Theoretical” curve which was formed by combining the theoretical equation relating the outer actuator to the inner actuator (Equation 2.9) with the best-fit equation relating the inner actuator displacement and the measured voltage (Equation 2.8). The resulting equation is as follows:

$$k = 5 + 2\sqrt{3^2 - 1.74\left(\frac{1}{V}\right) + 0.166\sqrt{\frac{1}{V}}} \quad (2.10)$$

Where k is in cm. This relationship can be used to control the actuator. Deviations between the theoretical model and measured relationship can be attributed to several causes. First, the theoretical model is based on a geometric shape with straight edges. In practice, the

actuator chambers are curved, so the sides of the outer actuator are not perfectly vertical. This leads to a reduction in the outer actuator length as compared to what is predicted by the model, and indeed this can be observed in Figure 2.18(b). Second, the dimensions of the fabricated actuator differed slightly from the intended lengths due to variations in manufacturing, leading to additional errors. In Figure 2.18(c), we observe a maximum error of 8% comparing the theoretical equation to the experimental fit, which occurs at a voltage of 0.6.

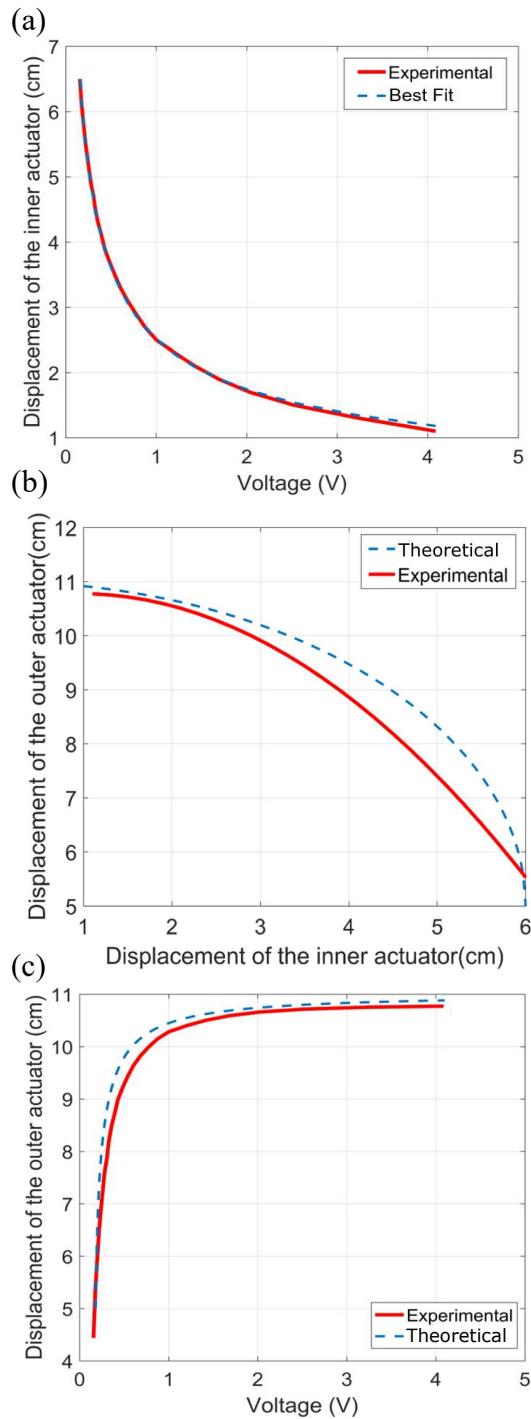


Figure 2.18: The experimental plot to compare with between distance of the outer actuator and displacement of the inner actuator, (a) The relationship between the inner actuator and voltage, (b) The relationship between the inner actuator and the outer actuator, (c) The relationship between the outer actuator and voltage.

Furthermore, actuator cycling tests were performed with the results described in Figure 2.18 below. The actuator was tested for long cycles, and particular cycling plot was shown to monitor inner actuator length and pressure in detail. During the cycling test, the actuator shows stable distance readings for the inner actuator around 6cm and constant pressure at 33kPa.

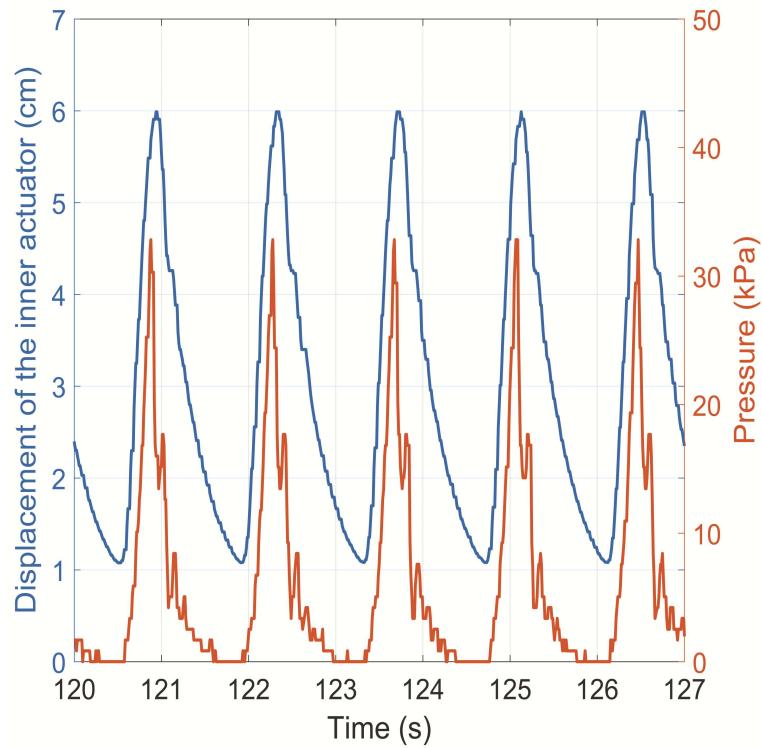


Figure 2.19: The cycling test of the actuator including the integrated electronics.

Chapter 3

Pneumatic Elbow Exoskeleton

We next designed a novel soft exoskeleton for an elbow joint using a manufacturing process and theory similar to that of the pneumatic actuator. We present the design of the exoskeleton and the modified manufacturing process, leaving the evaluation of the exoskeleton for future study. As shown in Figure 3.1, the soft exoskeleton is made completely of fabric with the exception of the tube fittings. This design attribute gives the exoskeleton intrinsic compliance and the ability to conform to the body.

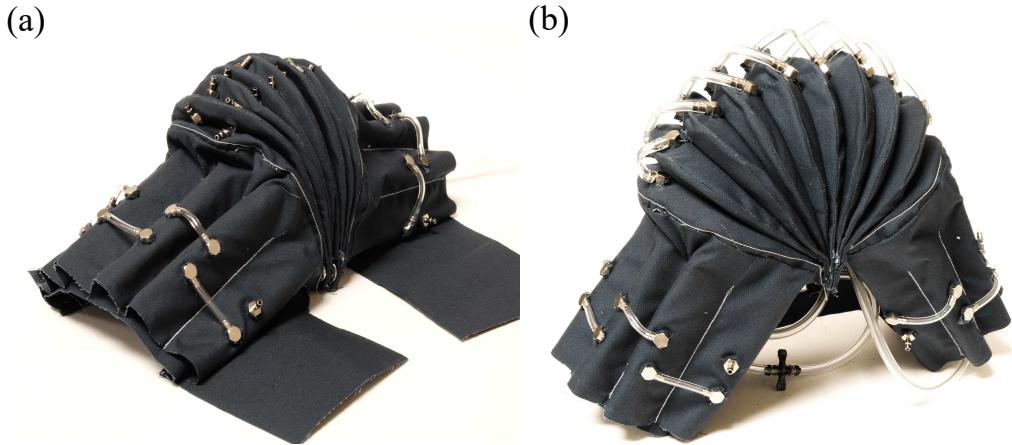


Figure 3.1: (a) A novel soft pneumatic exoskeleton for elbow joint in the initial state. (b) A novel soft pneumatic exoskeleton for elbow joint when it is inflated.

We modified our original fabrication process detailed in Chapter 2 to make the exoskeleton (Figures 3.2, 3.3, and 3.4). The manufacturing process can be separated into three major steps: the process for making two support structures of the exoskeleton (Figure 3.2), the actuated region (Figure 3.3), and assembling all the parts of the exoskeleton (Figure 3.4). The reason for dividing the fabrication process into three main processes is due to the fabric's single sided coating, which allows for bonding using heat. Furthermore, following the process, we modularized the exoskeleton into three main parts to make repairs easier and reduce manufacturing time.

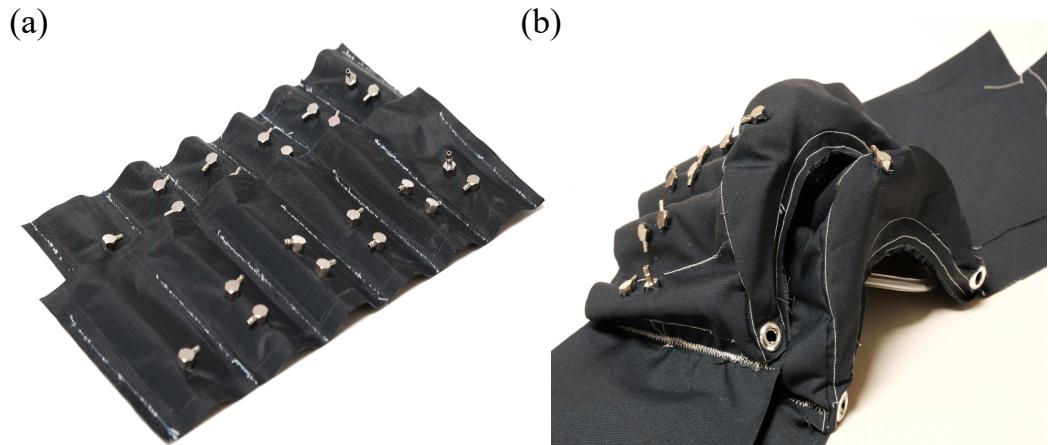


Figure 3.2: Two support structures of the exoskeleton.

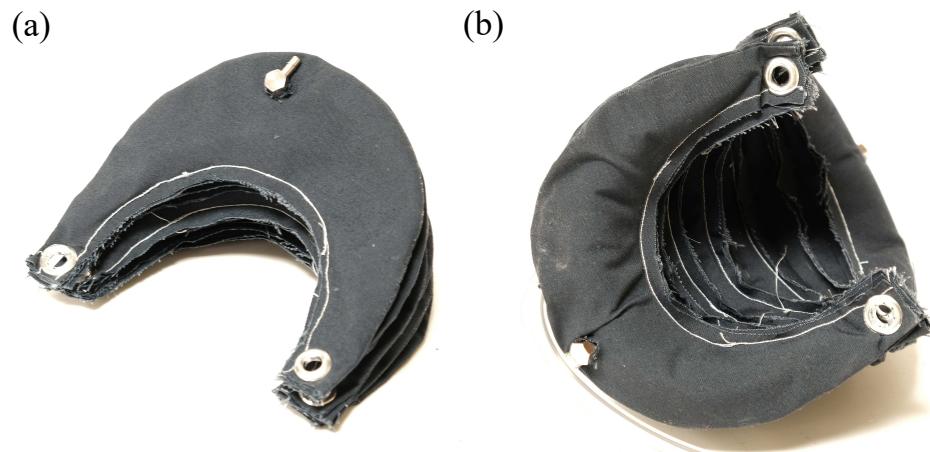


Figure 3.3: The main actuated region of the exoskeleton.



Figure 3.4: All parts of the exoskeleton.

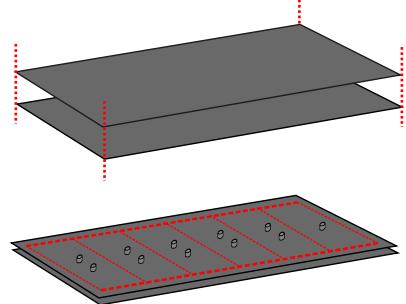
In the first step, shown in Figure 3.5, fabrics are bonded together with a heat sealer in a pattern indicated by the dashed lines in the lower portion of Step 1.1. In Step 1.2, an outer fabric layer is sewn onto the coated fabrics in the pattern shown by the dashed lines.

In the second step, we use the same process to make the actuated region using heat, and a sewing machine. The actuated region is formed by first bonding the fabrics with the soldering iron in the pattern shown by the dashed lines, sewing along the dashed lines, and then bonding the chambers together with thermal adhesive film placed in the pattern shown by the solid colored area.

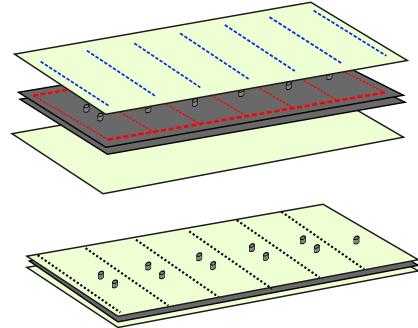
In the last step, the three segments of the exoskeleton are bonded together with thermal adhesive film placed in the pattern shown by the solid shaded area.

1. Design supporting structures

1. Align two coated fabrics and bond specific areas by a heat sealer

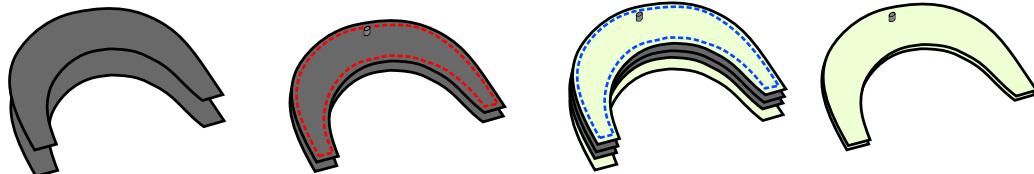


2. Sew outer fabrics and coated fabrics

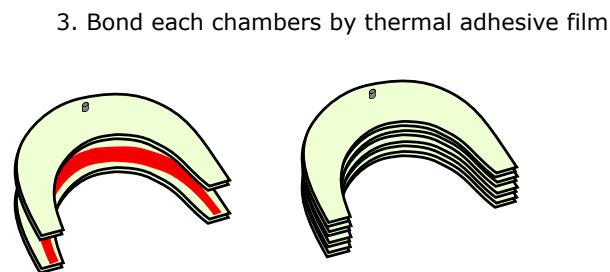


2. Design the actuated region

1. Align two coated fabrics and bond specific areas by a soldering iron



2. Sew outer fabrics and coated fabrics



3. Assemble all structures

1. Bond all part of exoskeleton using thermal adhesive film

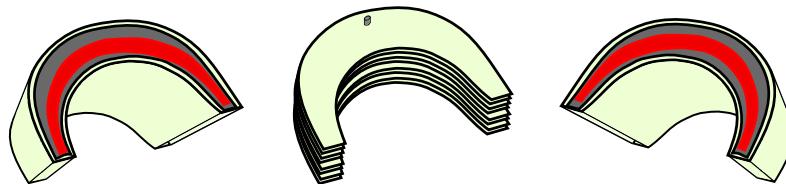


Figure 3.5: A manufacturing process for the arm exoskeleton based on the manufacturing system of the submitted paper.

The exoskeleton has many advantages compared to conventional exoskeletons and other pneumatic exoskeletons: extremely light weight, low material cost, and modularized design for easy repair. In a preliminary test, the exoskeleton generated force and torque when the angle was between 0 and 95 degrees as measured from a straight line (arm fully extended). The angular range over which the actuator can operate can be changed by varying the size and number of the actuated chambers. In this preliminary work, the force generation capability of the exoskeleton was not quantified; this is appropriate for future work.

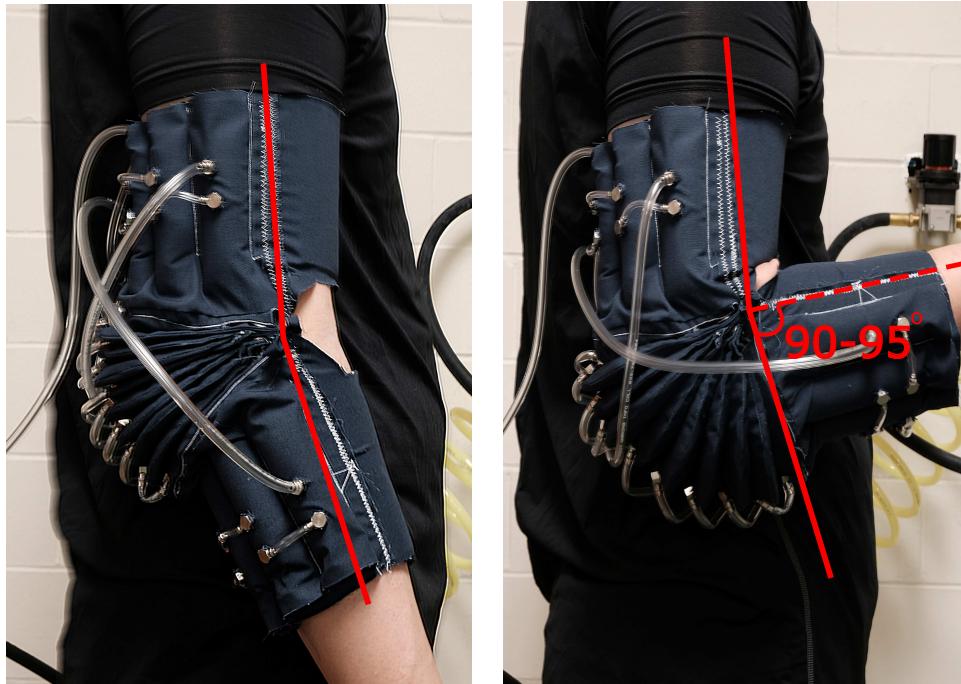


Figure 3.6: Photos of the exoskeleton on an arm demonstrating the range of motion.



Figure 3.7: Additional photos of the exoskeleton on an arm.

Chapter 4

Conclusion

In this paper we described a novel pneumatic artificial muscle actuator using soft materials for exoskeleton projects. Compared to traditional pneumatic actuators and even the latest soft actuators proposed recently, the novel actuator has many benefits. In particular, its greatest advantage is that we can design the actuator for a specific job requiring certain forces and contraction ratios. In order to quantify the benefits, tests depending on various actuators with different sizes were performed. The actuator can be designed to create various forces and exhibit contraction ratios from 40~65%. Furthermore, electronics can be integrated into the actuator, allowing it to be controlled directly.

We also presented an arm exoskeleton for the elbow joint that was made almost completely of fabric. Compared to the conventional exoskeleton, it has some benefits: low material cost, light weight for the portion worn on the arm, and intrinsic compliance. It was able to

provide force to the elbow from 0 to 95 degrees.

In the future, a variety of the pneumatic actuators will be investigated to determine our technique's possibilities. Furthermore, pneumatic source and electronics will be researched to control the soft arm exoskeleton.

Chapter 5

Bibliography

Bibliography

- [1] S. Balasubramanian, R. Wei, M. Perez, B. Shepard, E. Koeneman, J. Koeneman, and J. He, “Rupert: An exoskeleton robot for assisting rehabilitation of arm functions,” in *2008 Virtual Rehabilitation*, pp. 163–167, Aug 2008.
- [2] F. Sup, H. A. Varol, J. Mitchell, T. J. Withrow, and M. Goldfarb, “Preliminary evaluations of a self-contained anthropomorphic transfemoral prosthesis,” *IEEE/ASME Transactions on Mechatronics*, vol. 14, pp. 667–676, Dec 2009.
- [3] A. B. Zoss, H. Kazerooni, and A. Chu, “Biomechanical design of the berkeley lower extremity exoskeleton (bleex),” *IEEE/ASME Transactions on Mechatronics*, vol. 11, pp. 128–138, April 2006.
- [4] S. Sanan, P. S. Lynn, and S. T. Griffith, “Pneumatic torsional actuators for inflatable robots,” *Journal of Mechanisms and Robotics*, vol. 6, no. 3, p. 031003, 2014.
- [5] <http://www.roamrobotics.com/>.
- [6] G. Belforte, G. Eula, A. Ivanov, and A. L. Visan, “Bellows textile muscle,” *The Journal of The Textile Institute*, vol. 105, no. 3, pp. 356–364, 2014.
- [7] D. Yang, M. S. Verma, J.-H. So, B. Mosadegh, C. Keplinger, B. Lee, F. Khashai, E. Lossner, Z. Suo, and G. M. Whitesides, “Buckling pneumatic linear actuators inspired by muscle,” *Advanced Materials Technologies*, vol. 1, no. 3, 2016.
- [8] Z. Wang, P. Polygerinos, J. T. B. Overvelde, K. C. Galloway, K. Bertoldi, and C. J. Walsh, “Interaction Forces of Soft Fiber Reinforced Bending Actuators,” *IEEE/ASME Transactions on Mechatronics*, vol. PP, dec 2016.
- [9] B. Mosadegh, P. Polygerinos, C. Keplinger, S. Wennstedt, R. F. Shepherd, U. Gupta, J. Shim, K. Bertoldi, C. J. Walsh, and G. M. Whitesides, “Pneumatic networks for soft robotics that actuate rapidly,” *Advanced Functional Materials*, vol. 24, no. 15, pp. 2163–2170, 2014.
- [10] B. Davies, “A review of robotics in surgery,” *Proceedings of the Institution of Mechanical Engineers, Part H: Journal of Engineering in Medicine*, vol. 214, no. 1, pp. 129–140, 2000.

- [11] A. Tapus, M. J. Mataric, B. Scassellati, S. Member, and B. Scassellati, “The Grand Challenges in Socially Assistive Robotics,” *Robotics and Automation*, vol. 14, no. 1, pp. 1–7, 2007.
- [12] S. Seok, A. Wang, M. Y. M. Chuah, D. J. Hyun, J. Lee, D. M. Otten, J. H. Lang, and S. Kim, “Design principles for energy-efficient legged locomotion and implementation on the mit cheetah robot,” *IEEE/ASME Transactions on Mechatronics*, vol. 20, pp. 1117–1129, June 2015.
- [13] D. Rus and M. T. Tolley, “Design, fabrication and control of soft robots,” *Nature*, vol. 521, no. 7553, pp. 467–475, 2015.
- [14] S. Kim, C. Laschi, and B. Trimmer, “Soft robotics: A bioinspired evolution in robotics,” *Trends in Biotechnology*, vol. 31, no. 5, pp. 287–294, 2013.
- [15] A. Kristoffersson, S. Coradeschi, and A. Loutfi, “A review of mobile robotic telepresence,” *Advances in Human-Computer Interaction*, vol. 2013, 2013.
- [16] R. Bogue, “Exoskeletons and robotic prosthetics: a review of recent developments,” *Industrial Robot: An International Journal*, vol. 36, no. 5, pp. 421–427, 2009.
- [17] A. M. Dollar and H. Herr, “Lower Extremity Exoskeletons and Active Orthoses:Challenges and State-of-the-Art,” *IEEE Transactions on Robotics*, vol. 24, no. 1, pp. 144–158, 2008.
- [18] H. S. Lo and S. Q. Xie, “Exoskeleton robots for upper-limb rehabilitation: State of the art and future prospects,” *Medical Engineering and Physics*, vol. 34, no. 3, pp. 261–268, 2012.
- [19] K. A. Shorter, J. Xia, E. T. Hsiao-Wecksler, W. K. Durfee, and G. F. Kogler, “Technologies for powered ankle-foot orthotic systems: Possibilities and challenges,” *IEEE/ASME Transactions on Mechatronics*, vol. 18, no. 1, pp. 337–347, 2013.
- [20] Ching-Ping Chou and B. Hannaford, “Measurement and modeling of McKibben pneumatic artificial muscles,” *IEEE Transactions on Robotics and Automation*, vol. 12, no. 1, pp. 90–102, 1996.
- [21] C. S. Kothera, M. Philen, and B. Tondu, “Modelling of the mckibben artificial muscle: A review,” *Journal of Intelligent Material Systems and Structures*, vol. 23, no. 3, pp. 225–253, 2012.
- [22] F. Daerden and D. Lefeber, “Pneumatic artificial muscles: actuators for robotics and automation,” *European journal of mechanical and environmental engineering*, vol. 47, no. 1, pp. 11–21, 2002.

- [23] S. Davis, N. Tsagarakis, J. Canderle, and D. G. Caldwell, “Enhanced modelling and performance in braided pneumatic muscle actuators,” *The International Journal of Robotics Research*, vol. 22, no. 3-4, pp. 213–227, 2003.
- [24] B. Tondu and P. Lopez, “Modeling and control of McKibben artificial muscle robot actuators,” *IEEE Control Systems Magazine*, vol. 20, no. 2, pp. 15–38, 2000.
- [25] S. Davis and D. G. Caldwell, “Braid effects on contractile range and friction modeling in pneumatic muscle actuators,” *The International Journal of Robotics Research*, vol. 25, no. 4, pp. 359–369, 2006.
- [26] M. Doumit, A. Fahim, and M. Munro, “Analytical modeling and experimental validation of the braided pneumatic muscle,” *IEEE Transactions on Robotics*, vol. 25, no. 6, pp. 1282–1291, 2009.
- [27] F. Daerden and D. Lefeber, “The concept and design of pleated pneumatic artificial muscles.,” *International Journal of Fluid Power*, vol. 2, no. 3, pp. 41–50, 2001.
- [28] F. Daerden, D. Lefeber, B. Verrelst, and R. Van Ham, “Pleated pneumatic artificial muscles: compliant robotic actuators,” in *Intelligent Robots and Systems, 2001. Proceedings. 2001 IEEE/RSJ International Conference on*, vol. 4, pp. 1958–1963, IEEE, 2001.
- [29] D. Villegas, M. Van Damme, B. Vanderborght, P. Beyl, and D. Lefeber, “Third Generation Pleated Pneumatic Artificial Muscles for Robotic Applications: Development and Comparison with McKibben Muscle,” *Advanced Robotics*, vol. 26, no. 11-12, pp. 1205–1227, 2012.
- [30] B. Vanderborght, B. Verrelst, R. Van Ham, M. Van Damme, R. Versluys, and D. Lefeber, “Treadmill walking of the pneumatic biped Lucy: Walking at different speeds and step-lengths,” *International Applied Mechanics*, vol. 44, no. 7, pp. 830–837, 2008.
- [31] P. Beyl, M. Van Damme, R. Van Ham, B. Vanderborght, and D. Lefeber, “Pleated pneumatic artificial muscle-based actuator system as a torque source for compliant lower limb exoskeletons,” *IEEE/ASME Transactions on Mechatronics*, vol. 19, no. 3, pp. 1046–1056, 2014.
- [32] P. Beyl, M. Van Damme, R. Van Ham, B. Vanderborght, and D. Lefeber, “Design and Control of a Lower Limb Exoskeleton for Robot-assisted Gait Training,” *Appl. Bionics Biomechanics*, vol. 6, no. 2, pp. 229–243, 2009.
- [33] B. Tondu, S. Ippolito, J. Guiochet, and A. Daidie, “A seven-degrees-of-freedom robot-arm driven by pneumatic artificial muscles for humanoid robots,” *The International Journal of Robotics Research*, vol. 24, no. 4, pp. 257–274, 2005.

- [34] A. J. Veale, S. Q. Xie, and I. A. Anderson, “Modeling the Peano fluidic muscle and the effects of its material properties on its static and dynamic behavior,” *Smart Materials and Structures*, vol. 25, no. 6, p. 065014, 2016.
- [35] Y.-L. Park, J. Santos, K. G. Galloway, E. C. Goldfield, and R. J. Wood, “A soft wearable robotic device for active knee motions using flat pneumatic artificial muscles,” in *Robotics and Automation (ICRA), 2014 IEEE International Conference on*, pp. 4805–4810, IEEE, 2014.
- [36] R. Niiyama, D. Rus, and S. Kim, “Pouch motors: Printable/inflatable soft actuators for robotics,” in *Robotics and Automation (ICRA), 2014 IEEE International Conference on*, pp. 6332–6337, IEEE, 2014.
- [37] R. Niiyama, X. Sun, C. Sung, B. An, D. Rus, and S. Kim, “Pouch motors: Printable soft actuators integrated with computational design,” *Soft Robotics*, vol. 2, no. 2, pp. 59–70, 2015.
- [38] F. Ilievski, A. D. Mazzeo, R. F. Shepherd, X. Chen, and G. M. Whitesides, “Soft robotics for chemists,” *Angewandte Chemie*, vol. 123, no. 8, pp. 1930–1935, 2011.
- [39] F. Connolly, P. Polygerinos, C. J. Walsh, and K. Bertoldi, “Mechanical programming of soft actuators by varying fiber angle,” *Soft Robotics*, vol. 2, no. 1, pp. 26–32, 2015.
- [40] E. Origami, “Programmable paper-elastomer composites as pneumatic actuators martinez, ramses v.; fish, carina r.; chen, xin; whitesides, george m,” *Advanced Functional Materials*, vol. 22, no. 7, pp. 1376–1384, 2012.
- [41] J. R. Oliver, R. R. Neurgaonkar, A. P. Moffatt, M. Khoshnevisan, and J. G. Nelson, “Piezoelectric energy harvester and method,” 2002.
- [42] P. Ouyang, W. Zhang, and M. Gupta, “A new compliant mechanical amplifier based on a symmetric five-bar topology,” *Journal of Mechanical Design*, vol. 130, no. 10, p. 104501, 2008.
- [43] Y. Mengüç, Y.-L. Park, E. Martinez-Villalpando, P. Aubin, M. Zisook, L. Stirling, R. J. Wood, and C. J. Walsh, “Soft wearable motion sensing suit for lower limb biomechanics measurements,” in *Robotics and Automation (ICRA), 2013 IEEE International Conference on*, pp. 5309–5316, IEEE, 2013.